In Vitro Study of the Proteolytic Degradation of *Antheraea pernyi* Silk Fibroin

Paola Taddei,[†] Takayuki Arai,[‡] Alessandra Boschi,[§] Patrizia Monti,[†] Masuhiro Tsukada,[‡] and Giuliano Freddi*[,§]

Dipartimento di Biochimica "G. Moruzzi", Sezione di Chimica e Propedeutica Biochimica, Centro di Studio sulla Spettroscopia Raman, Università di Bologna, via Belmeloro 8/2, 40126 Bologna, Italy, National Institute of Agrobiological Sciences, Oowashi 1-2, Tsukuba, Ibaraki 305-8634, Japan, and Stazione Sperimentale per la Seta, via G. Colombo 83, 20133 Milano, Italy

Received August 31, 2005; Revised Manuscript Received November 4, 2005

In this study, *Antheraea pernyi* silk fibroin (Ap-SF) films were incubated with Protease Type XXI from *Streptomyces griseus*, at 37 °C, to investigate the degradation behavior in an in vitro model system. The enzyme-resistant fractions of Ap-SF films and the soluble peptides formed by proteolytic degradation were collected at specified times, from 1 to 17 days, and analyzed by high performance liquid chromatography, differential scanning calorimetry, FT-Raman, and FT-IR spectroscopy. Proteolysis resulted in extensive weight loss and progressive fragmentation of films, especially at long degradation times. A range of soluble peptides was formed by proteolysis. By high performance-size exclusion chromatography it was found that their average molecular weight changed with the time of incubation. The chemical analysis of the enzyme-resistant fraction of Ap-SF films at different times of degradation indicated that the proteolytic attack preferentially occurred in the less ordered Gly rich sequences and that the contribution of the Ala rich crystalline regions to the composition of biodegraded films became progressively larger. Accordingly, DSC and spectroscopic results showed an enhancement of the crystalline character of the biodegraded films. From the behavior of the most important thermal transitions, it was deduced that the α-helix domains probably represent the most enzyme-resistant fraction. The in vitro approach used in the present study seems to be a valid tool for studying the rate and mechanism of degradation of Ap-SF films and of other biopolymers of potential biomedical utility.

1. Introduction

The silk spun by the larvae of both domestic (i.e., *Bombyx mori*) and wild silkworm species (i.e., *Antheraea pernyi*, *Philosamia c. ricini*, etc.) is both a renewable fibrous biopolymer and one of the most valuable starting materials for the textile industry. As a textile fiber, silk by itself is thermo-insulating, well tolerated by the skin, and capable of maintaining an optimally moisturized environment. Silk is also a versatile and chemically reactive biopolymer endowed with excellent intrinsic biological properties. Previous studies have demonstrated that silk has an excellent biocompatibility.[1−6] Moreover, silk can be easily functionalized, and its structure and morphology can be modulated to match a wide range of working requirements.[3] Because of these reasons, in recent years, the unique chemical, mechanical, and biological properties of silk have made this protein polymer a highly attractive candidate for the development of innovative, knowledge-based multifunctional materials aimed at different end-uses, such as technical textiles and biomedical devices (i.e., scaffolds for tissue engineering).

Silk fibers have been studied as the starting material for preparing various sorts of biomedical devices, such as polymer−hydroxyapatite composites for bone regeneration,[7] wire ropes for the replacement of the anterior cruciate ligament,[8] and novel sutures and gauzes for treating skin burn wounds.[9] Silk films, which are easily prepared by casting aqueous silk protein solutions at room temperature, are highly attractive for their discrete permeability to oxygen and water vapor.[10] Like fibers, films can support cell adhesion and growth, and their use to manufacture scaffolds for the regeneration of skin, bone, and other tissues has been proposed.[11,12]

Currently, efforts are aimed at adjusting the structure of biomaterials to their required functions. Making available novel compatible and functionalized biomaterials addressing a broad range of biomedical needs is a crucial scientific and technological challenge. In this context, the well established range of properties of silk strongly recommends the use of this biopolymer as a means to develop innovative biomaterials intended for clinical applications. To act as an optimal biomaterial, silk should be integrated into the regenerating tissue and stay well tolerated there for the time needed to perform the required function. This comment addresses the important issue of the degree of biostability of silk. Altman et al.[3] recently reviewed studies on the degradation behavior of silk sutures and concluded that silk in fiber form can be considered a slowly degradable material in vivo, though the rate of degradation may be highly variable depending on the properties of the material itself, as well as on the chemical and biochemical environment of the site of implantation.

Gaining a clear understanding of the relationship between structure, processing, and degradability is a prerequisite for designing silk-based devices for biomedical applications. Studies on the degradation behavior of *B. mori* silk fibers,[13,14] films,[13] and porous sheets[15] exposed to the action of different proteases in vitro have recently been reported. It was observed that the

* Corresponding author. Tel.: +39 02 2665990. Fax: +39 02 2362788. E-mail: freddi@ssiseta.it.
[†] Universitá di Bologna.
[‡] Institute of Agrobiological Sciences.
[§] Stazione Sperimentale per la Seta.

10.1021/bm0506290 CCC: $33.50
Published on Web 12/15/2005

rate of degradation significantly differed between fibers and regenerated silk materials, like films or porous sheets. The latter degraded more quickly, through a mechanism which involved the preferential attack to the amorphous domains.[13,15] Fibers exhibited a loss of mechanical integrity, accompanied by a concomitant loss of mass which resulted from both increased fragmentation and decrease of silk filament diameter over the time of exposition to the proteolytic enzyme.[14]

These results highlight that in vitro studies greatly contributed to improve the understanding of the kinetics and mechanism of the enzyme-mediated degradation of *B. mori* silk fibroin. Comparatively few studies have been carried out on the degradation behavior of silk fibroin obtained from the wild silkworm *A. pernyi*. Tsukada[16] studied the structural characteristics of the enzyme-resistant fraction of *A. pernyi* silk fibroin films subjected to proteolytic degradation with α-chymotrypsin and alkaline phosphatase. However, no details were reported on the kinetics and mechanism of the degradation process. Similar to *B. mori*, *A. pernyi* silk fibroin can also be considered a potentially attractive biopolymer for developing biomedical applications owing to its good interactions with living cells.[17] The aim of the present study is to investigate the degradation behavior of *A. pernyi* silk fibroin films exposed to the proteolytic action of a bacterial protease according to an in vitro biodegradation model already developed for *B. mori* silk fibroin.[13] Biodegraded silk fibroin films and degradation products were examined by high performance liquid chromatography (HPLC), differential scanning calorimetry (DSC), Fourier Transform infrared (FT-IR) and FT-Raman spectroscopy with the aim to characterize their chemical and physical properties and to contribute new insight into the kinetics and mechanism of the degradation process.

2. Materials and Methods

2.1. Materials. 2.1.1. Silk Substrate. *A. pernyi* silk fibroin (Ap-SF) films were prepared as described elsewhere.[18] The liquid silk collected from the posterior portion of the silk gland was gently dispersed into deionized water until a final concentration of about 0.3 w%. The aqueous SF solution was cast on a polyethylene plate, at ambient temperature. Films were treated with a 50 v% water−methanol solution for 30 min, and dried at 85 °C for 3 h before incubation with protease.

2.1.2. Enzyme. Protease Type XXI from *Streptomyces griseus* (Sigma Prod. No. P-0652), dissolved in 50 mM potassium phosphate pH 7.5, was used for the in vitro biodegradation tests.[13] Protease activity was determined according to the Sigma Quality Control Test Procedure, by using casein (Sigma Prod. No. C-7078) as a substrate. One unit is defined as the amount of protease needed to hydrolyze casein to produce color equivalent to 1.0 μmole/min of tyrosine at pH 7.5 at 37 °C (color by Folin & Ciocalteu's reagent, Sigma Prod. No. F-9252).

2.1.3. In Vitro Degradation System. Ap-SF films were incubated in the following conditions: material-to-liquor ratio 5 mg of SF/mL; enzyme-to-substrate ratio 1 U/mg of SF; temperature 37 °C; time from 1 to 17 days. Blank samples were immersed in the buffer alone, without enzyme. Each test sample contained an equivalent mass of silk (≅15 mg). Tests were performed in duplicate. The enzyme solution was changed for the first time after 2 days and then every 3 days (at least 80% of the initial enzyme activity was retained after 3 days of incubation). At each change, the solid Ap-SF film was rinsed with water and immersed into a fresh buffered solution of the protease to continue the biodegradation. The solution containing soluble peptides was pooled with washing water and freeze-dried before subsequent analysis.

2.2. Measurements. 2.2.1. Weight Loss. To determine the weight loss, Ap-SF films were taken out from the solution, rinsed with water, dried at 105 °C, and weighed. Weight loss was expressed as percentage of the initial dry weight. Results are the average of duplicate tests.

2.2.2. Amino Acid Analysis. The amino acid composition of the films was determined by acid hydrolysis with 6 N HCl, at 105 °C, for 24 h, under vacuum. Free amino acids were analyzed by HPLC (AccQ-Tag Method, Waters). Eluate was detected at 254 nm. Samples were analyzed in duplicate. The Amino Acid Standard H kit (Pierce) was used for calibration.

2.2.3. High Performance-Size Exclusion Chromatography. High performance-size exclusion chromatography (HP-SEC) analysis of soluble peptides was performed with a Waters Alliance chromatographic system. Freeze-dried soluble Ap-SF peptides were dissolved with 2 mL of elution buffer (50 mM sodium phosphate buffer, pH 7.2, containing 0.15 M KCl), filtered, and loaded onto a Protein Pak-60 column (Waters). The injection volume was 50 μL, and the flow rate was 0.5 mL/min. Eluate was detected at 254 nm with a Waters 2996 Photodiode Array Detector. All samples were analyzed in duplicate. The molecular weight calibration curve, obtained by using the Gel Filtration Calibration Kits (Pharmacia Biotech), was used to calculate the cumulative weight fraction distribution of soluble peptides.[19]

2.2.4. FT-IR Spectroscopy. The FT-IR spectra of the dried films were measured in the ATR mode with a Nexus spectrometer Thermo Nicolet, equipped with a ZnSe ATR cell mod. Smart Performer.

2.2.5. FT-Raman Spectroscopy. The Raman spectra of the dried films were measured on a Bruker IFS66 spectrometer equipped with a FRA-106 FT-Raman module and a cooled Ge-diode detector. The spectral resolution was 4 cm^{-1}. The excitation source was a Nd^{3+}-YAG laser (1064 nm) in the backscattering (180°) configuration. The Raman spectra were normalized to the alanine bands, because the cleaved fragments can be considered not to contain a significant amount of alanine; Raman intensities were calculated as peak heights.

2.2.6. Differential Scanning Calorimetry. Differential scanning calorimetry (DSC) measurements were performed with a DSC-30 instrument (Mettler Toledo), from room temperature to 500 °C, at a heating rate of 10 °C/min, on 2−3 mg samples. The open aluminum cell was swept with N_2 during the analysis.

3. Results and Discussion

3.1. Kinetics of Proteolytic Degradation of Ap-SF Films and Chemical Composition of the Enzyme-Resistant Fraction. Upon incubation with protease, the weight of Ap-SF films progressively decreased over the time period examined (Figure 1A). Best fitting of data points was obtained with a third-degree polynomial curve ($R^2 = 0.99$) The total weight loss accounted for about 70 w% in 17 days. Comparatively similar results were reported for *B. mori*-SF films[13] and porous sheets,[15] although the kinetics of biodegradation followed different trends. The three-dimensional structure of Ap-SF films remained almost intact during the first few days of proteolysis, showing only signs of surface erosion. As the incubation time increased the films appeared more extensively degraded and at the end they were recovered as finely powdered material. The weight loss of blank Ap-SF films, i.e., incubated in the buffer without protease, was negligible (≤2 w%). The original film texture resisted under the wet test conditions, owing to the annealing effect of the preliminary treatment with 50 v% aqueous methanol.[20]

The enzyme-resistant fraction of biodegraded Ap-SF films was recovered and the chemical composition was determined (Table 1). The amino acid composition of Ap-SF is characterized by a large amount of alanine.[21] Poly$(Ala)_n$ sequences are reported to form the basic structure of the crystalline regions.[22,23] Ala rich regions alternate with Gly rich regions which contain a variety of other amino acids the most abundant of which are Ser, Tyr, Asp, Arg, and Trp.[23] Upon proteolytic degradation,

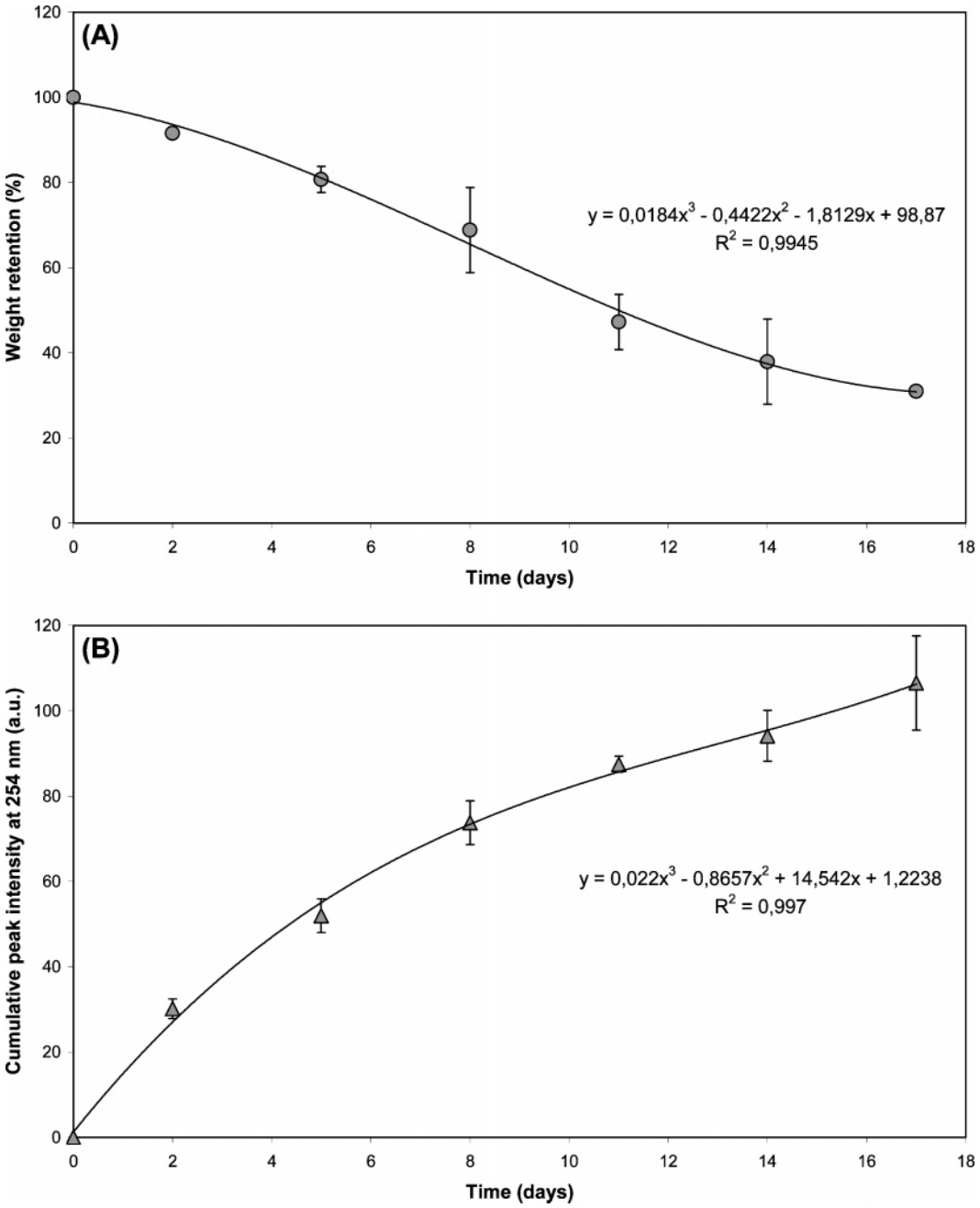

Figure 1. (A) Weight of the enzyme-resistant fractions of Ap-SF films and (B) cumulative amount of soluble peptides released into the incubation bath as a function of the time of degradation with protease.

Table 1. Amino Acid Composition ± Associated Error (mol %) of Biodegraded Ap-SF Films

amino acid	control[a]	5 days	11 days	17 days
Ala	38.89 ± 0.35	39.45 ± 0.40	41.24 ± 0.39	44.83 ± 0.49
Gly	29.71 ± 0.31	31.15 ± 0.42	30.56 ± 0.51	29.24 ± 0.38
Ser	10.56 ± 0.11	11.04 ± 0.10	11.25 ± 0.08	11.06 ± 0.12
Tyr	5.64 ± 0.05	5.56 ± 0.06	4.85 ± 0.04	4.10 ± 0.04
Asp+Glu	6.85 ± 0.07	6.15 ± 0.05	5.64 ± 0.08	5.36 ± 0.05
Lys+His+Arg	4.03 ± 0.03	3.45 ± 0.07	2.78 ± 0.05	2.56 ± 0.05
others	4.33 ± 0.07	3.20 ± 0.08	3.68 ± 0.07	2.85 ± 0.06
weight retention (%)	98.2 ± 0.5	80.7 ± 3.1	47.2 ± 4.5	31.0 ± 0.5

[a] Incubated for 17 days with buffer alone.

the amino acid composition of the enzyme-resistant fraction showed significant changes: the Ala percentage increased gradually, the Gly and Ser percentages remained almost unchanged, while the percentages of Tyr, acidic, and basic amino acids decreased. These results provide deeper insight into the kinetics and mechanism of the proteolytic attack, which preferentially occurred in the Gly rich domains. These findings are not surprising. Although the random coil content in methanol−water treated Ap-SF films is hard to be quantified by DSC and spectroscopic measurements (see below), the Gly

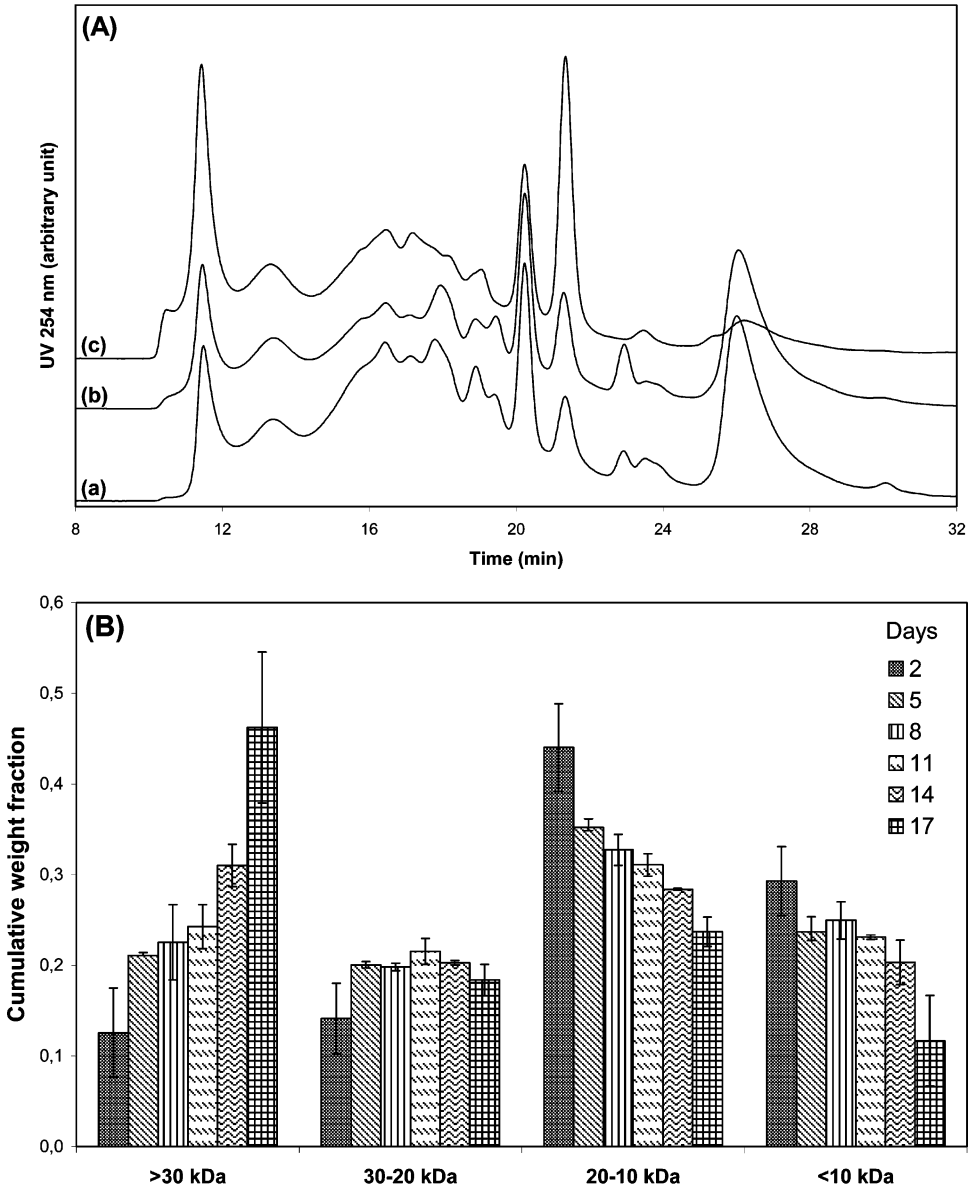

Figure 2. (A) HP−SEC profiles of soluble peptides obtained at 5 (a), 11 (b), and 17 (c) days of degradation. (B) Changes in the weight fraction of soluble peptides, grouped into MW classes, as a function of the time of degradation.

rich sequences are expected to be definitely less ordered than the poly(Ala)$_n$ domains. ^{13}C cross-polarization magic angle spinning NMR measurements performed on water-methanol treated Ap-SF films showed that the fractions of Ala residues in β-sheet, α-helix, and random coil conformation are 70%, 20%, and 10%, respectively.[24] The β-sheet and α-helix structures are located in the poly(Ala)$_n$ sequences, whereas the Ala residues with random coil conformation were assigned to those in the Gly rich domains. All Gly residues were reported to take random coil conformation upon water−methanol treatment; nearly all Tyr residues take the same conformation. As regards Ser, 60% of these residues take β-sheet structure, 20% α-helix (mainly in Asp-Ser-Ala sequences) and 20% random coil.

On this basis, it can be affirmed that, not unexpectedly, the enzyme could penetrate more easily into the less ordered Gly rich regions, cleave the sensitive peptide bonds ,and release free soluble peptides. Since the less ordered Gly rich sequences were preferentially cleaved, the contribution of Ala to the composition of degraded films increased, as observed from the data of Table 1. These features were also confirmed by the spectroscopic analysis of the enzyme-resistant fractions.

3.2. Molecular Weight Distribution of Soluble Ap-SF Peptides. Soluble peptides formed by proteolytic degradation of Ap-SF films were recovered and analyzed by HP−SEC. The cumulative amount of soluble peptides, expressed as total intensity of the chromatographic peaks at 254 nm, increased with the biodegradation time, displaying a trend complementary to that of weight loss (Figure 1B). Figure 2A shows a series of chromatographic profiles of the hydrolysis products obtained at different biodegradation times (5th, 11th, and 17th day). The pattern is typical of a complex mixture of peptides widely differing in size, with molecular weight (MW) ranging from about 35 to 2 kDa.

Changes in the chromatographic pattern were observed in the peptide mixtures collected at different biodegradation times. To verify whether these changes had a systematic trend, the weight fraction of peptides falling within defined MW classes was calculated from the chromatographic peaks and plotted as a function of the biodegradation time. The histograms of Figure 2B show that the fraction of high MW peptides (>30 kDa) increased sharply with the time of incubation, i.e. increasingly larger peptides were released into the solution when the films

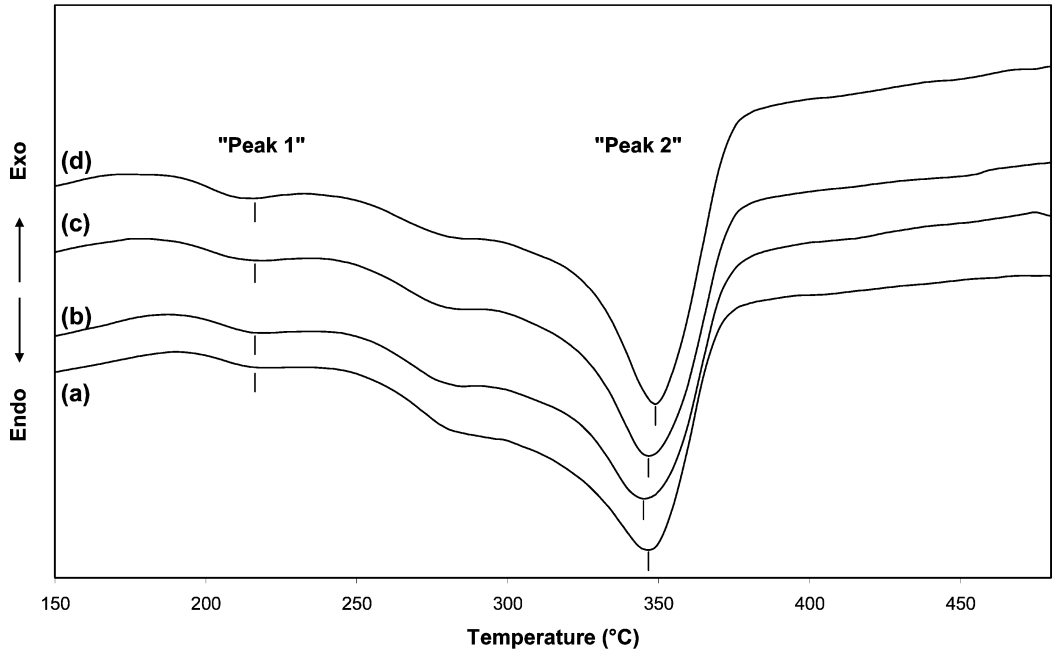

Figure 3. DSC curves of control Ap-SF films treated with buffer alone for 17 days (a), and after incubation with protease for 2 (b), 8 (c), and 14 (d) days.

were in a more advanced biodegradation stage. The fraction of peptides with MW in the 20−30 kDa remained almost constant, while the other two groups of medium-to-small MW peptides (10−20 kDa and <10 kDa) decreased with increasing the contact time between Ap-SF films and protease.

The protease used in this work hydrolyzes peptide bonds on the carboxyl side of Glu and Asp (according to Sigma specifications). With reference to the gene-derived primary structure of Ap-SF,[23] Glu is mainly located close to the N- and C-terminuses, while at least one Asp residue falls in every Gly rich region which alternates regularly with the Ala rich regions. The presence of several Asp residues along the chain length means that the number of cleavage sites potentially available is quite large and that formation of medium-to-small size peptides is expected from enzymatic hydrolysis. On the contrary, the size of soluble peptides covered a wide MW range; large-size peptides were present at different biodegradation stages; and the peptide pattern changed as a function of the biodegradation time. For a peptide bond to be broken, it must be accessible to the protease.[13,15] Several morphological and structural factors limited the real accessibility of cleavage sites in the system under study. Among them were (a) the compact texture of crystallized Ap-SF films, (b) the extent of swelling in the aqueous medium, (c) the vicinity of cleavage sites to the β-sheet crystalline domains, (d) the three-dimensional arrangement of SF chains in the less ordered domains, and (e) the fraction of cleavage sites exposed to the film surface. As biodegradation progressed, some of these factors probably became less restrictive, because films were more fragmented, restrictions to swelling were partially removed, and previously unexposed surfaces became accessible to the protease. This may account for the changes in soluble peptide properties, as demonstrated by the HP−SEC results. However, it appears very difficult to correlate the observed changes with specific factors, and to model the hydrolytic attack of protease toward Ap-SF films, especially because the system was further complicated by the fact that soluble peptides themselves became a substrate of proteolytic attack.

3.3. Thermal Characterization of Biodegraded Ap-SF Films. Figure 3 shows the DSC thermograms of Ap-SF films blank-treated and subjected to biodegradation for different times. The whole samples examined displayed a similar thermal behavior, with an initial broad endotherm at <100 °C, attributed to evaporation of moisture (not shown in the figure), followed by a typical high-temperature pattern which consisted in a weak and broad endotherm peaking at about 216 °C (peak 1), and a strong endotherm at about 350 °C (peak 2), preceded by a lower-temperature shoulder. The transition at above 300 °C is attributed to melting/decomposition of Ap-SF with unoriented β-sheet crystalline structure.[25,26] The endotherm at 216 °C, which is often present in solution cast native Ap-SF films annealed in water-methanol solution, is related to the presence of residual α-helix crystalline domains.[25]

The thermal pattern was not significantly affected by biodegradation. However, the intensity of the main thermal transitions changed in a way that suggested some relationship with the hydrolytic action of protease. In fact, as listed in Table 2, the intensity of peaks 1 and 2 tended to increase with increasing the biodegradation time, and the temperature of peak 2 slightly shifted to higher values. With reference to the above-reported attributions, it appears that the contribution of the crystalline domains, either β-sheet or α-helix, to the thermal behavior of Ap-SF films increased with increasing the time of biodegradation. This agrees with the chemical results previously discussed, indicating that the amorphous domains of Ap-SF film were preferentially degraded by the protease. However, the trend of the ratio between the ΔH values of the two thermal transitions ($\Delta H_\beta/\Delta H_\alpha$, see Table 2) indicates that also β-sheet structure underwent a certain degradation. In other words, the decrease of $\Delta H_\beta/\Delta H_\alpha$ ratio during degradation can be interpreted according to Tsukada:[16] the α-helix domain represents the fraction more resistant to the enzyme. Actually, the presence of α-helix has been reported to contribute to the chemical stability of fibroin.[27] At this purpose, it can be recalled that the presence of the Asp-Ser sequences at the N-terminal of the α-helix structure of poly(Ala)$_n$ domains have been speculated to strengthen this structure. Therefore, it can be hypothesized that these specific Asp residues could be the least probably attacked by the enzyme.

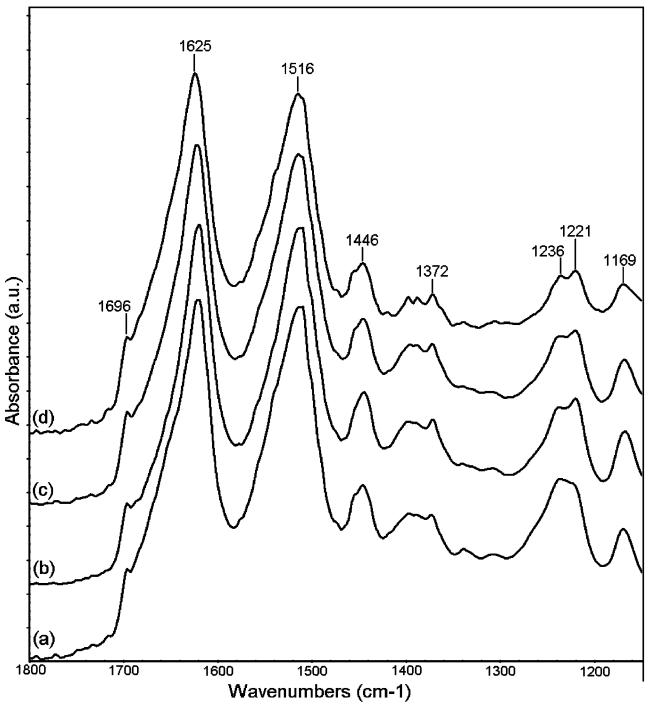

Figure 4. FT-IR spectra of control Ap-SF films treated with buffer alone for 17 days (a), and after incubation with protease for 5 (b), 11 (c), and 17 (d) days.

Table 2. Peak Temperature and Enthalpy of Biodegraded Ap-SF Films

	peak 1	peak 2		
sample	ΔH_α (J/g)	ΔH_β (J/g)	temperature (°C)	$\Delta H_\beta/\Delta H_\alpha$
control[a]	4.19	165.6	347.5	39.5
2 days	5.62	174.7	346.7	31.1
8 days	6.66	185.0	347.1	27.8
14 days	8.03	193.1	349.3	24.1

[a] Incubated for 17 days with buffer alone.

3.4. Spectroscopic Characterization of Biodegraded Ap-SF Films. It has been shown that Ap-SF films cast from aqueous solution contain variable proportions of α-helix and random coil conformations, which can be converted into the *β*-sheet conformation (i.e., the structure present in cocoon fibers) by changing drying temperature and drying rate[28] or by chemical-physical treatments, such as heating[20,26] and immersion in water−methanol solutions.[18] Figure 4 shows the IR spectra of Ap-SF films blank-treated and exposed to biodegradation for different times in the 1800−1100 cm^{-1} wavenumber range. The three main conformationally sensitive amide bands, with peak maxima falling at 1696 and 1625 cm^{-1} (amide I), 1516 cm^{-1} (amide II), and 1236 and 1221 cm^{-1} (amide III), can be observed. This spectral pattern is characteristic of Ap-SF films with prevailing *β*-sheet conformation.[29] At this purpose, it must be observed that the complex profile of the amide bands indicates the presence of other conformations besides *β*-sheet.[30]

Some spectral changes of the enzyme resistant fractions suggest that the crystalline character of Ap-SF films was enhanced upon biodegradation. The typical feature confirming this trend is the increase in relative intensity of the amide III component at 1221 cm^{-1} with respect to that at 1236 cm^{-1}. Actually, Frushour and Koenig[31] have observed that in the IR spectrum of *β*-sheet poly(Ala)$_n$ obtained by stretching α-helical fibers, the 1220 cm^{-1} band is very strong. Moreover, it has been suggested that in poly(Ala)$_n$ the bands at about 1220 and 1240 cm^{-1} are due to the splitting of amide III in the antiparallel *β*-sheet conformation, without excluding the possibility that the higher wavenumber band could be due to the Amide III mode of the disordered chain.[32] Also the spectral variations in the 1420−1350 cm^{-1} range (prevalently CH_3 and H^α bending) are consistent with conformational changes, as previously suggested.[29,32,33] Similar spectral variations were reported in differently heated Ap-SF films.[26]

Figure 5 shows the Raman spectra of Ap-SF films blank-treated and after treatment with protease for 5 and 17 days. According to our previous Raman studies,[18,20] the position of the amide I and III modes at 1669 and 1242−1230 cm^{-1}, and the presence of the bands at 1094, 1071, and 965 cm^{-1} attributable to vibrations of Ala rich segments of the fibroin chain,[31,32] reveals that the untreated film had a prevailing *β*-sheet conformation. However, also in this case, it must be observed that the complex profile of the Amide bands indicates the presence of other conformations besides *β*-sheet.[34]

The trend of the full-width at half-maximum (fwhm) of the amide I band at 1669 cm^{-1} shows that the enzymatic treatment enhanced the crystalline character of the Ap-SF film. It is interesting to note that the fwhm of the amide I band quickly decreased until 11 days of degradation, and after that, it remained nearly constant (Figure 6). This trend can be explained in terms of the morphology of the Ap-SF film. In the first 11 days, degradation involved the peptide sequences most sensitive to the proteolytic attack (definitely the amorphous domains and, on the basis of the DSC results, the most exposed *β*-sheet domains). The degradation of these sequences proceeded until they were exhausted and after that the fwhm of the Amide I band did not sensibly decrease since degradation involved the more crystalline and slow-degrading *β*-sheet domains.

Upon proteolytic degradation other Raman bands showed significant changes in relative intensity and width. Those attributed to Tyr at 1615, 1265, 1208, 1173, 853, 829, and 644 cm^{-1},[34,35] to Trp at 1615, 1550, 1011, and 760 cm^{-1},[36] and to Asp[37] at 1416 cm^{-1} progressively decreased in intensity during degradation. Weakening of spectral intensity was observed in the 1400−1300 cm^{-1} range as well, probably due to contributions arising from both Trp and Asp.[36,37] Also the band at 1032 cm^{-1} (skeletal νC−C)[38] became weaker. For a more quantitative evaluation, some intensity ratios were identified as marker of degradation. Figure 7A reports the trend of the intensity ratio between the bands at 644 cm^{-1} (Tyr) and 906 cm^{-1} (Ala band, taken as internal standard because the cleaved fragments can be considered not to contain a significant amount of alanine). It is interesting to note that, during degradation, I_{644}/I_{906} has the same trend as the Tyr content determined by HPLC (see Table 1); that is, it remained nearly constant until 8 days and then noticeably decreased. Moreover, it must be observed that the Raman spectrum of Tyr presents a doublet at 853 and 829 cm^{-1} attributed to Fermi resonance between the ring breathing vibration and the overtone of an out-of-plane ring bending vibration of Tyr.[34,39] The value of the I_{853}/I_{829} intensity ratio is sensitive to the hydrogen-bonding state of the Tyr phenoxyl group and has been extensively used as an indicator of Tyr interactions in globular proteins, of their assemblies, and of their degree of exposure to water.[40] It is worth noting that the ratio calculated from the spectrum is a mean value, since it averages the state of the whole Tyr residues present in the protein. If the Tyr residue is buried, the phenolic OH group acts as a strong hydrogen-bond donor to an electronegative acceptor (such as carboxyl oxygen) and the I_{853}/I_{829} ratio achieves its minimum value of about 0.3.[40] When the Tyr residue is exposed on the

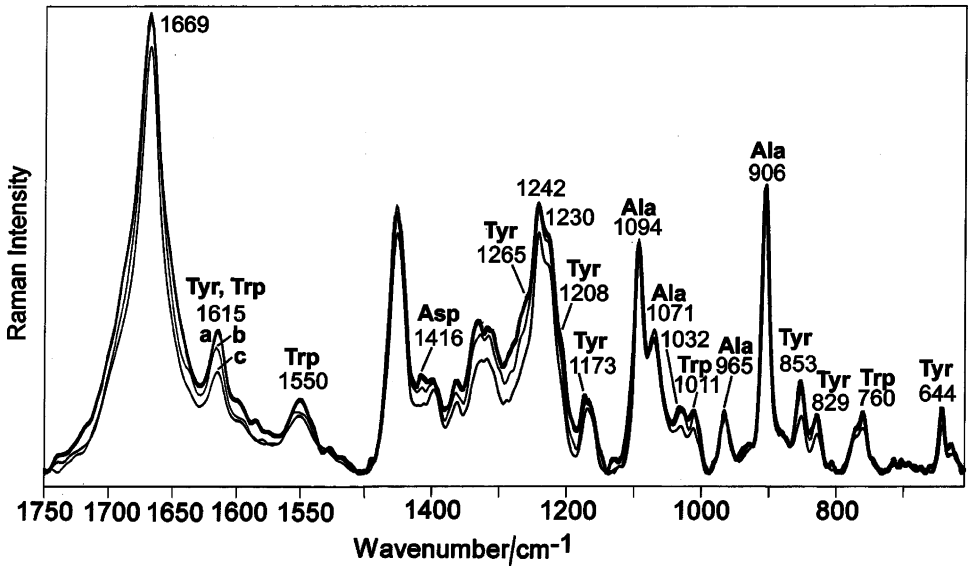

Figure 5. FT-Raman spectra of control Ap-SF films treated with buffer alone for 17 days (a), and after incubation with protease for 5 (b) and 17 (c) days. The spectra are baseline corrected and normalized to Ala bands.

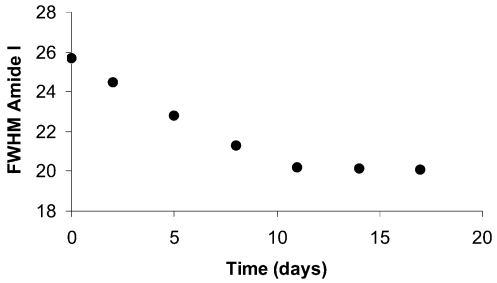

Figure 6. Trend of the full-width at half-maximum (fwhm) of the Raman amide I band of Ap-SF films during degradation.

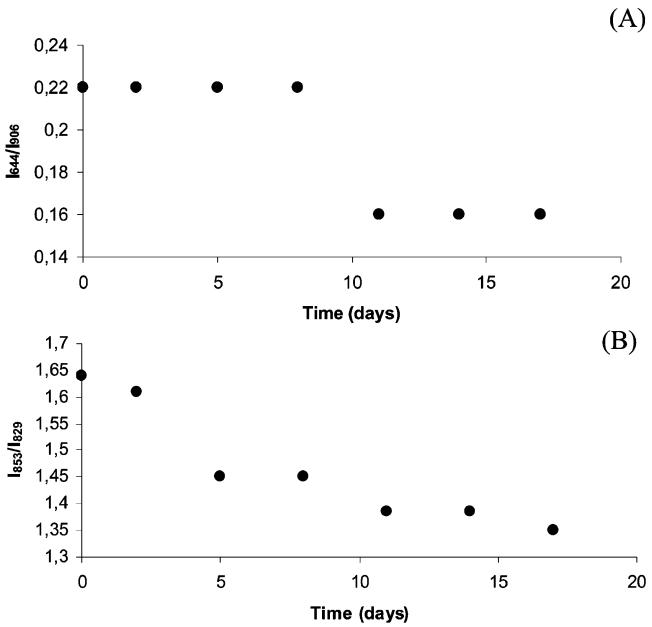

Figure 7. Trend of the I_{644}/I_{906} (A) and I_{853}/I_{829} (B) Raman intensity ratios during degradation of Ap-SF films exposed to protease.

surface of a protein in aqueous solution, the phenolic OH group acts as both a donor and an acceptor of moderate hydrogen bonds and the I_{853}/I_{829} is approximately 1.25.[40] This correlation was refined on the basis of the results obtained on filamentous virus capsids[41−44] and SF with Silk I structure,[45] which showed that the I_{853}/I_{829} ratio can markedly exceed the latter value. This has been interpreted as indicative of a highly hydrophobic local environment for Tyr residues, a state not represented in any previously studied globular protein.

The trend of the I_{853}/I_{829} intensity ratio during degradation (Figure 7B) appears particularly interesting if compared with the trend of I_{644}/I_{906}. As can be easily seen, the I_{853}/I_{829} ratio sensibly decreased after 5 days of degradation, i.e., before the decreases of I_{644}/I_{906} and Tyr content. This result indicates that, at this stage, although degradation had not yet caused a decrease of the Tyr content, it induced a rearrangement of the fibroin chain characterized by a more "buried" state of Tyr. On the other hand, at 11 days of degradation, when the Tyr content begins to decrease (Table 1 and Figure 7B), the I_{853}/I_{829} decrease can be explained also assuming that a certain amount of 'exposed' Tyr residues, initially present in the domains more accessible to protease, were lost with the peptide fragments removed by proteolytic cleavage.

The Raman results highlight that the bands assigned to the amino acid residues comprising the Gly rich sequences became less intense, confirming that the proteolytic attack preferentially occurred in the less ordered Gly rich sequences.

4. Conclusions

The results here reported allow to conclude that Ap-SF films are susceptible to proteolytic attack. Proteolysis resulted in extensive weight loss and formation of a range of soluble peptides whose MW changed with the time of incubation. The chemical analysis of the enzyme resistant Ap-SF films at different times of degradation indicated that the proteolytic attack preferentially occurred in the less ordered Gly rich sequences and that the contribution of the Ala rich crystalline regions to the composition of biodegraded films became progressively larger. In confirmation, DSC, and spectroscopic results showed an enhancement of the crystalline character of biodegraded films. The thermal findings suggested that the α-helix domain probably represented the structural fraction more resistant to the proteolytic attack. The in vitro approach used in the present study seems a valid tool for studying the biodegradation rate and mechanism of Ap-SF materials. A long-

term study of the enzymatic degradation of Ap-SF fibers is in progress and further improvements of this in vitro approach may definitely lead to develop a model system suitable for evaluating the biodegradation behavior of silk biomaterials. In fact, knowledge of the rate and mechanism, as well as of the effect of the proteolytic attack is a key factor for designing high-performing silk-based biomedical devices.

Acknowledgment. This work was supported by 60% grants from MIUR.

References and Notes

(1) Santin, M.; Motta, A.; Freddi, G.; Cannas, M. In vitro evaluation of the inflammatory potential of the silk fibroin. *J. Biomed. Mater. Res.* **1999**, *46*, 382−389.

(2) Vollrath, F.; Barth, P.; Basedow, A.; Engstrom, W.; List, H. Local tolerance to spider silks and protein polymers in vivo. *In vivo* **2002**, *16*, 229−234.

(3) Altman, G. H.; Diaz, F.; Jakuba, C.; Calabro, T.; Horan, R. L.; Chen, J.; Lu, H.; Richmond, J.; Kaplan, D. L. Silk-based biomaterials. *Biomaterials* **2003**, *24*, 401−416.

(4) Panilaitis, B.; Altman, G. H.; Chen, J.; Jin, H. J.; Karageorgiou, V.; Kaplan, D. L. Macrophage response to silk. *Biomaterials* **2003**, *24*, 3079−3085.

(5) Yamada, H.; Igarashi, Y.; Takasu, Y.; Saito, H.; Tsubouchi, K. Identification of fibroin-derived peptides enhancing the proliferation of cultured human fibroblasts. *Biomaterials* **2004**, *25*, 467−472.

(6) Dal Pra, I.; Freddi, G.; Minic, J.; Chiarini, A.; Armato, U. *De novo* engineering of reticular connective tissue in vivo by silk fibroin nonwoven materials. *Biomaterials* **2005**, *26*, 1987−1999.

(7) Kikuchi, M.; Matsumoto, H. N.; Yamada, T.; Koyama, Y.; Takakuda, K.; Tanaka, J. Glutaraldehyde cross-linked hydroxyapatite/collagen self-organized nanocomposites. *Biomaterials* **2004**, *25*, 63−69.

(8) Altman, G. H.; Horan, R. L.; Lu, H. H.; Moreau, J.; Martin, I.; Richmond, J. C.; Kaplan, D. L. Silk matrix for tissue engineered anterior cruciate ligaments. *Biomaterials* **2002**, *23*, 4131−4141.

(9) Sugihara, A.; Sugiura, K.; Morita, H.; Ninagawa, T.; Tubouchi, K.; Tobe, R.; Izumiya, M.; Horio, T.; Abraham, N. G.; Ikehara, S. Promotive effects of a silk film on epidermal recovery from full-thickness skin wounds. *Proc. Soc. Exp. Biol. Med.* **2000**, *225*, 58−64.

(10) Minoura, N.; Tsukada, M.; Nagura, M. Physicochemical properties of silk fibroin membrane as a biomaterial. *Biomaterials* **1990**, *11*, 430−434.

(11) Sofia, S.; McCarthy, M. B.; Gronowicz, G.; Kaplan, D. L. Functionalized silk-based biomaterials for bone formation. *J. Biomed. Mater. Res.* **2001**, *46*, 139−148.

(12) Gotoh, Y.; Niimi, S.; Hayakawa, T.; Miyashita, T. Preparation of lactose-silk fibroin conjugates and their application as a scaffold for hepatocyte attachment. *Biomaterials* **2004**, *25*, 1131−1140.

(13) Arai, T.; Freddi, G.; Innocenti, R.; Tsukada, M. Biodegradation of *Bombyx mori* silk fibroin fibers and films. *J. Appl. Polym. Sci.* **2004**, *91*, 2383−2390.

(14) Horan, R. L.; Antle, K.; Collette, A. L.; Wang, Y.; Huang, J.; Moreau, J. E.; Volloch, V.; Kaplan, D. L.; Altman, G. H. In vitro degradation of silk fibroin. *Biomaterials* **2005**, *26*, 3385−3393.

(15) Li, M.; Ogiso, M.; Minoura, N. Enzymatic degradation behavior of porous silk fibroin sheets. *Biomaterials* **2003**, *24*, 357−365.

(16) Tsukada, M. Structure of the enzyme-resistant fraction of tussah silk (*Antheraea pernyi*) fibroin. *J. Polym. Sci.: Part B: Polym. Phys.* **1988**, *26*, 949−952.

(17) Minoura, N.; Aiba, S.; Higuchi, M.; Gotoh, Y.; Tsukada, M.; Imai, Y. Attachment and growth of fibroblast cells on silk fibroin. *Biochem. Biophys. Res. Commun.* **1995**, *208*, 511−516.

(18) Tsukada. M.; Freddi, G.; Monti, P.; Bertoluzza, A.; Kasai, N. Structure and molecular conformation of tussah silk fibroin films: effect of methanol. *J. Polym. Sci.: Part B: Polym. Phys.* **1995**, *33*, 1995−2001.

(19) Yau, W. W.; Kirkland, J. J.; Bly, D. D. *Modern size exclusion liquid chromatography*: *practice of gel permeation and gel filtration chromatography*; Wiley-Interscience: New York, 1979.

(20) Tsukada, M.; Freddi, G.; Kasai, N.; Monti, P. Structure and molecular conformation of tussah silk fibroin films treated with water-methanol solutions: dynamic mechanical and thermomechanical behavior. *J. Polym. Sci.: Part B: Polym. Phys.* **1998**, *36*, 2717−2724.

(21) Tsukada, M.; Freddi, G.; Gotoh, Y.; Kasai, N. Physical and chemical properties of tussah silk fibroin films. *J. Polym. Sci.: Part B: Polym. Phys.* **1994**, *32*, 1407−1412.

(22) Fraser, R. D. B.; MacRae, T. P. *Conformation in fibrous proteins and related synthetic polypeptides*; Academic Press: New York, 1973.

(23) Sezutsu, H.; Yukuhiro, K. Dynamic rearrangement within the *Antheraea pernyi* silk fibroin gene is associated with four types of repetitive units. *J. Mol. Evol.* **2000**, *51*, 329−338.

(24) Nakazawa, Y.; Asakura, T. High resolution ^{13}C CP/MAS NMR study on structure and structural transition of *Antheraea pernyi* silk fibroin containing poly(L-alanine) and Gly rich regions. *Macromolecules* **2002**, *35*, 2393−2400.

(25) Tsukada, M. Structural changes induced in tussah silk (*Antheraea pernyi*) fibroin films by immersion in methanol. *J. Polym. Sci.: Polym. Phys. Ed.* **1986**, *24*, 1227−1232.

(26) Freddi, G.; Monti, P.; Nagura, M.; Gotoh, Y.; Tsukada, M. Structure and molecular conformation of tussah silk fibroin films: effect of heat treatment. *J. Polym. Sci.: Part B: Polym. Phys.* **1997**, *35*, 841−847.

(27) Tsukada, M.; Nagura, M.; Ishikawa, H. Structural changes in poly(L-alanine) induced by heat treatment. *J. Polym. Sci.: Part B: Polym. Phys.* **1987**, *25*, 1325−1329.

(28) Tsukada, M. Effect of the drying rate on the structure of tussah silk (*Antheraea pernyi*) fibroin. *J. Polym. Sci.: Polym. Phys. Ed.* **1986**, *24*, 457−460.

(29) Taddei, P.; Monti P.; Freddi, G.; Arai, T.; Tsukada, M. IR study on the binding mode of metal cations to chemically modified *Bombyx mori* and Tussah silk fibres. *J. Mol. Struct.* **2003**, *651*−*653*, 433−441.

(30) Stuart, B. *Biological applications of Infrared Spectroscopy*; Wiley: Chichester, U.K., 1997.

(31) Frushour, B. G.; Koenig, J. L. Raman spectroscopic study of mechanically deformed poly-L-alanine. *Biopolymers* **1974**, *13*, 455−474.

(32) Moore, W. H.; Krimm, S. Vibrational analysis of peptides, polypeptides, and proteins. II. β-poly(L-alanine) and β-poly(L-alanylglycine). *Biopolymers* **1976**, *15*, 2465−2483.

(33) Mathur, A. B.; Tonelli, A.; Rathke, T.; Hudson, S. The dissolution and characterization of *Bombyx mori* silk fibroin in calcium nitrate-methanol solution and the regeneration of films. *Biopolymers* **1997**, *42*, 61−74.

(34) Tu, A. T. *Raman spectroscopy in biology: Principles and applications*; Wiley: Chichester, U.K., 1982.

(35) Takeuchi, H.; Watanabe, N.; Satoh, Y.; Harada, H. Effects of hydrogen bonding on the tyrosine Raman bands in the 1300−1150 cm^{-1} region. *J. Raman Spectrosc.* **1989**, *20*, 233−237.

(36) Miura, T.; Takeuki, H.; Harada, I. Tryptophan Raman bands sensitive to hydrogen bonding and side chain conformation. *J. Raman Spectrosc.* **1989**, *20*, 667−671.

(37) Lopez Navarrete, J. T.; Hernandez, V.; Ramirez, F. J. Ir and Raman spectra of L-aspartic acid and isotopic derivatives. *Biopolymers* **1994**, *34*, 1065−1077.

(38) Edwards, H. G. M.; Farwell, D. W. Raman spectroscopic studies of silk. *J. Raman Spectrosc.* **1995**, *26*, 901−909.

(39) Harada, I.; Takeuchi, H. Raman and ultraviolet resonance Raman spectra of proteins and related compounds. In *Spectroscopy of Biological Systems. Advances in Spectroscopy*; Clark, R. J. H., Hester, R. E., Eds.; John Wiley & Sons: New York, 1986; Vol. 13, pp 113−175.

(40) Siamwiza, M. N.; Lord, R. C.; Chen, M. C.; Takamatsu, T.; Harada, I.; Matsuura, H.; Shimanouchi, T. Interpretation of the doublet at 850 and 830 cm^{-1} in the Raman spectra of tyrosyl residues in proteins and certain model compounds. *Biochemistry* **1975**, *14*, 4870−4876.

(41) Overman, S. A.; Aubrey, K.; Vispo, N. S.; Cesareni, G.; Thomas, J. H., Jr. Novel tyrosine markers in Raman spectra of wild-type and mutant (Y21M and Y24M) Ff virions indicate unusual environments for coat protein phenoxyls. *Biochemistry* **1994**, *34*, 1039−1042.

(42) Wen, Z. Q.; Armstrong, A.; Thomas, G. J., Jr. Demonstration by ultraviolet resonance Raman spectroscopy of differences in DNA organization and interactions in filamentous viruses Pf1 and fd. *Biochemistry* **1999**, *38*, 3148−3156.

(43) Arp, Z.; Autrey, D.; Laane, J.; Overman, S. A.; Thomas, G. J., Jr. Tyrosine Raman signatures of the filamentous virus Ff are diagnostic

of non-hydrogen-bonded phenoxyls: demonstration by Raman and infrared spectroscopy of *p*-cresol vapor. *Biochemistry* **2001**, *40*, 2522−2529.

(44) Thomas, G. J., Jr. New structural insights from Raman spectroscopy of proteins and their assemblies. *Biopolymers (Biospectroscopy)* **2002**, *67*, 214−225.

(45) Taddei, P.; Asakura, T.; Yao, J.; Monti, P. Raman study of poly-(alanine-glycine)-based peptides containing tyrosine, valine and serine as model for the semicrystalline domains of *Bombyx mori* silk fibroin. *Biopolymers (Biospectroscopy)* **2004**, *75*, 314−324.

BM0506290